ACS Sustainable Chemistry & Engineering

pubs.acs.org/journal/ascecg

Research Article

Design and Optimization of the Direct Recycling of Spent Li-Ion Battery Cathode Materials

Panpan Xu, Zhenzhen Yang, Xiaolu Yu, John Holoubek, Hongpeng Gao, Mingqian Li, Guorui Cai, Ira Bloom, Haodong Liu, Yan Chen, Ke An, Krzysztof Z. Pupek, Ping Liu, and Zheng Chen*

Cite This: *ACS Sustainable Chem. Eng.* 2021, 9, 4543−4553

Read Online

ACCESS | Metrics & More | Article Recommendations | Supporting Information

ABSTRACT: Direct regeneration of spent Li-ion batteries based on the hydrothermal relithiation of cathode materials is a promising next-generation recycling technology. In order to demonstrate the feasibility of this approach at a large scale, we systematically design and optimize the process parameters to minimize both energy and raw material costs. Specifically, the effects of regenerative processing parameters on the composition, structure, and electrochemical performance of the regenerated cathode materials are investigated via systematic characterization and testing. From this analysis, it was found that the raw material costs can be substantially reduced by either replacing the typically employed 4 M LiOH solution by a cost-effective mixture of 0.1 M LiOH and 3.9 M KOH or recycling of the concentrated 4 M LiOH for continuous relithiation processes. Life cycle analysis suggests that this strategy results in reduced energy consumption and greenhouse gas emissions, leading to an increased potential revenue, particularly when compared with hydro- and pyrometallurgical recycling methods.

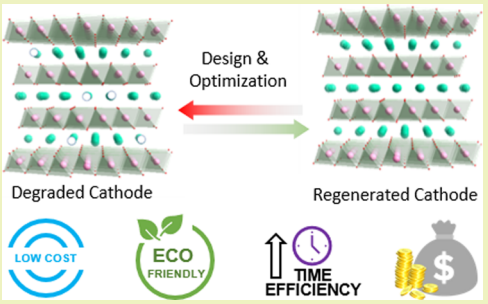

KEYWORDS: *spent Li-ion batteries, NCM cathode material, direct recycling, hydrothermal relithiation, process design and optimization*

INTRODUCTION

Li-ion batteries (LIBs) are widely applied in portable electronic devices, electric vehicles, and large-scale energy storage systems. Due to the increasing desire for clean and sustainable energy, it is projected that the global LIB production will reach ∼440 GWh by 2025.[1] At a typical life span of 5−10 years, a large quantity of LIBs will be retired in the next few years.[1] Without appropriate treatment strategies, these spent LIBs will pose a great challenge to our society. In this regard, recycling is regarded as an effective, closed-loop solution to mitigate environmental issues and reclaim valuable resources contained in spent LIBs.

Due to their high material value, the recycling of spent cathode materials has attracted intensive attention.[1−3] While pyro- and hydrometallurgy are commercialized in the recycling industry, they involve high-temperature smelting or usage of large amounts of acid and alkaline chemicals, increasing operation costs and posing a risk of secondary environmental pollution.[4,5] In addition, these strategies completely decompose the cathodes to their elemental products, resulting in a loss in total energy efficiency, as the cathode must then be remanufactured.[6,7] Therefore, an efficient yet green recycling approach is urgently needed to mitigate the aforementioned technical and environmental challenges.

Recently, our group and others have demonstrated a direct regeneration method based on hydrothermal relithiation, which can effectively recycle spent $LiCoO_2$ (LCO),[8,9] $LiNi_{0.33}Co_{0.33}Mn_{0.33}O_2$ (NCM111),[10] $LiNi_{0.5}Co_{0.2}Mn_{0.3}O_2$ (NCM523),[10,11] and $LiNi_{0.6}Co_{0.2}Mn_{0.2}O_2$ (NCM622)[12] cathodes back to a "pristine" state in terms of composition, structure, and electrochemical performance.[8,10,11] In this method, the spent cathode particles can be healed via hydrothermal relithiation (for composition recovery) followed by a short annealing step (for microstructure recovery) without destroying the cathode morphology. However, operation parameters involved in the direct regeneration process and their impact on the electrochemical performance of recycled cathodes have not yet to be systematically studied or optimized.

In order to demonstrate the technological and economic feasibility of the direct regeneration process at scale, we have performed such a process optimization, which is generally focused on the choice of regeneration solution composition. Particularly, it was found that LiOH (about $17/kg)[13] could be largely replaced by KOH (about $0.7/kg)[14] without any substantial negative effects on the performance of the regenerated materials. In a separate experiment, we also demonstrated the recyclability of the typically employed LiOH solution, yielding a continuous operation with improved

Received: December 11, 2020
Revised: February 13, 2021
Published: March 18, 2021

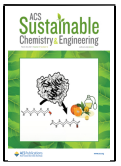

https://doi.org/10.1021/acssuschemeng.0c09017
ACS Sustainable Chem. Eng. 2021, 9, 4543−4553

efficiency. To further reduce the energy cost associated with the post-annealing step, LiOH salt was used to compensate for Li loss during microphase reconstruction, which allows for a lower annealing temperature compared to that used with Li_2CO_3. All of these strategies have the potential to significantly reduce regeneration costs compared to previous processes.[8,10] Life cycle analysis suggests that this direct recycling method is consistent with the "4H" principle of recycling, namely, high efficiency, high economic return, high environmental benefit, and high safety, demonstrating great industrial potential.

EXPERIMENTAL SECTION

Material Degradation. Degraded NCM111 (D-NCM111) with 10% Li loss was supplied by the Materials Engineering Research Facility (MERF) at the Argonne National Laboratory. Note that in real battery waste streams, there might be a large variety of cell types with different state-of-health. To avoid such complexity and really separately study the impact of the process parameters, here we chose chemically delithiated NCM111 as a model material for our study. To obtain D-NCM111, pristine NCM111 purchased from Toda America Inc. T-NCM111 was reacted with an aqueous solution of potassium persulfate. The material was then washed with water followed by acetonitrile before drying under vacuum at ambient temperature. This standard delithiated material was produced in a 1 kg single batch process and was used as our starting material.

Material Regeneration. In a typical process, 1 g of D-NCM111 was regenerated in two steps: hydrothermal relithiation and short annealing.[8,10] In the relithiation step, different hydrothermal temperatures of 160, 200, and 220 °C and different reaction times of 1, 2, 4, and 6 h at each temperature were explored. Various solution compositions for relithiation were studied as well. In addition to 4 M LiOH used in our previous work and that of others,[8−10,12] a mixed solution consisting of 0.1 M LiOH and 3.9 M KOH was used for relithiation. The sample hydrothermally relithiated at 220 °C for 2 h with 4 M LiOH was denoted as HT-NCM111.

The material after hydrothermal relithiation was washed with water two times to remove the residual LiOH on the cathode particles. The relithiated black powder was then dried in a vacuum oven at 120 °C overnight. The dried powder was then mixed with a small amount of excess Li_2CO_3 (~5 mol % excess) to explore the effect of annealing temperature and time. The mixture was annealed at temperatures of 550, 650, 750, and 850 °C. The effect of annealing time was investigated at 850 °C. Here, 1, 2, 4, and 6 h annealing times were used. Similarly, HT-NCM111 was also mixed with 5 mol % excess LiOH and annealed at temperatures ranging from 550 to 850 °C. The annealed sample was denoted as HS-NCM111. For a larger-scale test and demonstration, 10 g of D-NCM111 was subjected to hydrothermal relithiation at 220 °C for 2 h and annealing at 850 °C for 4 h with Li_2CO_3 as the Li source. The final product was denoted as R-NCM111-10 g.

Material Characterization. The chemical compositions of different cathode powders were determined by inductively coupled plasma mass spectrometry (ICP-MS for Li Ni, Co, and Mn) and inductively coupled plasma optical emission spectroscopy (ICP-OES for Li, Ni, Co, Mn, and K). The surface composition was characterized by X-ray photoelectron spectroscopy (XPS) measurements. XPS data was acquired using a PHI 5000 VersaProbe II system (Physical Electronics) attached to an argon-atmosphere glovebox. The base pressure was ~1×10^{-8} torr. The samples were placed in the XPS chamber by moving them through the glovebox (no air exposure). The spectra were obtained under the following conditions: 100 μm beam (25 W) with Al Kα radiation ($h\upsilon$ = 1486.6 eV), Ar^+-ion and electron beam sample neutralization, fixed analyzer transmission mode, and pass energy of 23.50 eV. The Shirley background data were subtracted from all spectra. The spectra were fitted to multiple Gaussian peaks by using the software package (Multipack) that Physical Electronics provided. The crystal structure was characterized by X-ray powder diffraction (XRD) employing Cu Kα radiation (Bruker D2 Phaser). Detailed lattice information was obtained by powder neutron diffraction (PND), which was performed in high-resolution mode ($\Delta d/d \approx 0.25\%$) for a duration of 2 h under the nominal 1.4 MW SNS operation, and then processed using VDRIVE software.[15] Rietveld refinement of the neutron diffractions was performed using GSAS software with EXPGUI interface.[16,17]

Electrochemical Characterization. Electrochemical performance of all the samples was evaluated by fabricating coin half-cells. The electrode was prepared using a typical slurry-coating method. Briefly, the slurry was made by mixing the cathode powder, conductive agent (Super P65), and polyvinylidene fluoride (PVDF) in a mass ratio of 8:1:1 in *N*-methyl-2-pyrrolidone (NMP) solvent. It was then coated onto aluminum foil before drying at 120 °C for 12 h in a vacuum oven. The dry laminate was punched and calendared. Coin cells were fabricated inside the glovebox using the above cathode laminate (mass loading of ~7 mg/cm^2); Li metal as the anode; and LP 40 (1 M $LiPF_6$ in ethylene carbonate/diethyl carbonate = 50:50 (v/v)) as the electrolyte. Cycling stability was tested with activation at a rate of C/10 for four cycles followed by 50 cycles at a rate of C/3 (Figure S1). Cyclic voltammetry (CV) tests were performed in a three-electrode system, which was composed of D-NCM111 as the working electrode, a platinum plate as the counter electrode, and Ag/AgCl electrode as the reference electrode.

Regression Analysis. Polynomials were fit to hydrothermal time and temperature and initial capacity data using a method based on Scheffé's statistics of mixtures ideas.[18,19] Originally developed, the statistics of mixtures model empirically fits a given property of the mixture using a polynomial to represent the linear and higher-order contributions of each component. One implicit assumption in this model is that $x_1 + x_2 + x_3 + ... + x_n = 1$, where x_n is the weight, mole, or volume fraction of each component. For the purposes of this work, this assumption was ignored. However, the representations of the contributions from the components were still used. From the standpoint of an empirical model, it should not matter how these contributions are represented if the representation makes chemical and/or mathematical sense.

For two independent variables, the general fitting polynomial was $y = a_1x_1 + a_2x_2 + a_{12}x_1x_2 + b_1x_1(x_1 - x_2) + b_2x_2(x_1 - x_2)$. Here, x_1 represents temperature in °C, and x_2 represents time in h. The a_nx_n terms represent the linear contributions to y, and the others represent the contributions of the interactions between time and temperature. The linear terms, $a_1x_1 + a_2x_2$, were always present in the polynomials.

A search algorithm for candidate polynomials was implemented in Visual Basic for Applications in Microsoft Excel. Here, robust linear regression was used to minimize the effect of noise in the data and Tukey's iterative, biweight function[20−22] with a tuning constant of 6 was used to weight the data. The goodness-of-fit, r^2, was calculated using the expressions given in eqs 1−3:

$$\mathrm{TSS} = \sum y^2 \tag{1}$$

$$\mathrm{RSS} = \sum (\hat{y} - y)^2 \tag{2}$$

$$r^2 = \frac{\mathrm{TSS} - \mathrm{RSS}}{\mathrm{TSS}} \tag{3}$$

where TSS is the total sum of squares, y is the experimentally observed value, RSS is the residual sum of squares, and $\hat{y}$ is calculated from the fit.[23]

The search process generated many polynomials. Candidate polynomials that represented the data with a value of $r^2 \geq 0.95$ were selected for further consideration. The following criteria were used to further limit the number of polynomials. (1) The polynomial had the fewest number of terms; the fit was overdetermined. (2) The standard error had to be 40% or less than the value of the parameter so that, at the 95% confidence level, the value of the fitting parameter would still be larger than twice of the standard error.

https://doi.org/10.1021/acssuschemeng.0c09017
ACS Sustainable Chem. Eng. 2021, 9, 4543−4553

RESULTS AND DISCUSSION

Overview of the Process Design Consideration. An overview of the process discussed above is shown schematically in Figure 1. Here, a lithium-deficient metal oxide was regenerated in two steps, hydrothermal relithiation (HT) and short annealing (SA). In the discussion below, we present our results from the investigation of the processing parameters in each step, including the lithium source, temperatures, and times in both steps. We show that, once optimized, the overall process yields a cathode that maintains the same crystal structure and electrochemical performance as pristine materials.

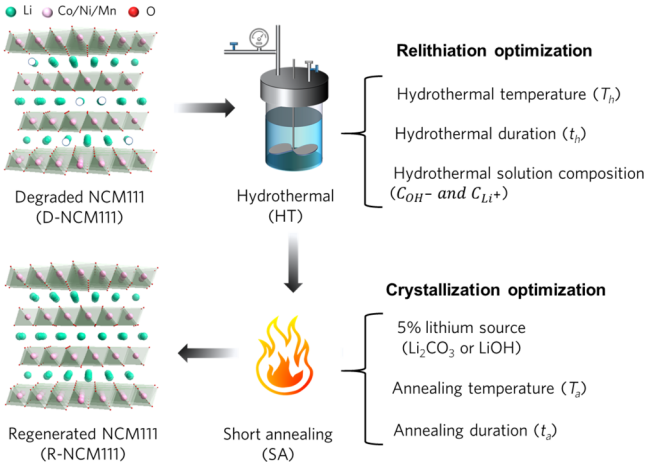

Figure 1. Overview of the process design consideration. Schematic illustration of hydrothermal relithiation-based direct regeneration of D-NCM111 and parameters involved in the hydrothermal relithiation and short annealing process.

Investigation of Temperature and Time of the Hydrothermal Relithiation Process. The effects of hydrothermal temperatures and relithiation times on the electrochemical performance of the regenerated materials were examined first. Here, D-NCM111 was relithiated at 160, 200, and 220 °C with 4 M LiOH for 1, 2, 4, and 6 h. When D-NCM111 was relithiated at 160 °C, the sample treated for 1 h showed an initial discharge capacity of 130 mAh/g at a C/3 rate (Figure S1a and Table S1) and retained only 81.5% of its initial capacity after 50 cycles. When the relithiation time was increased to 2 h, the initial capacity improved to 135 mAh/g and the capacity retention increased to 83.7%, which were further improved when relithiation time was increased, as shown in Table S1. When D-NCM111 was relithiated for 6 h, the capacity reached 147 mAh/g and the capacity retention increased to 85.0%. The treatment temperature was then increased to 200 °C (Figure S1b). At this temperature, the sample relithiated for 1 h exhibited an initial capacity and capacity retention of 147 mAh/g and 81.6% after 50 cycles, respectively. A similar improvement trend with the increase in relithiation time (Table S1) to that of samples relithiated at 160 °C was also observed, indicating that both the relithiation temperature and time are crucial. The temperature was then elevated to 220 °C. As shown in Figure S1c, an initial capacity of 149 mAh/g was produced after only 1 h of relithiation, but

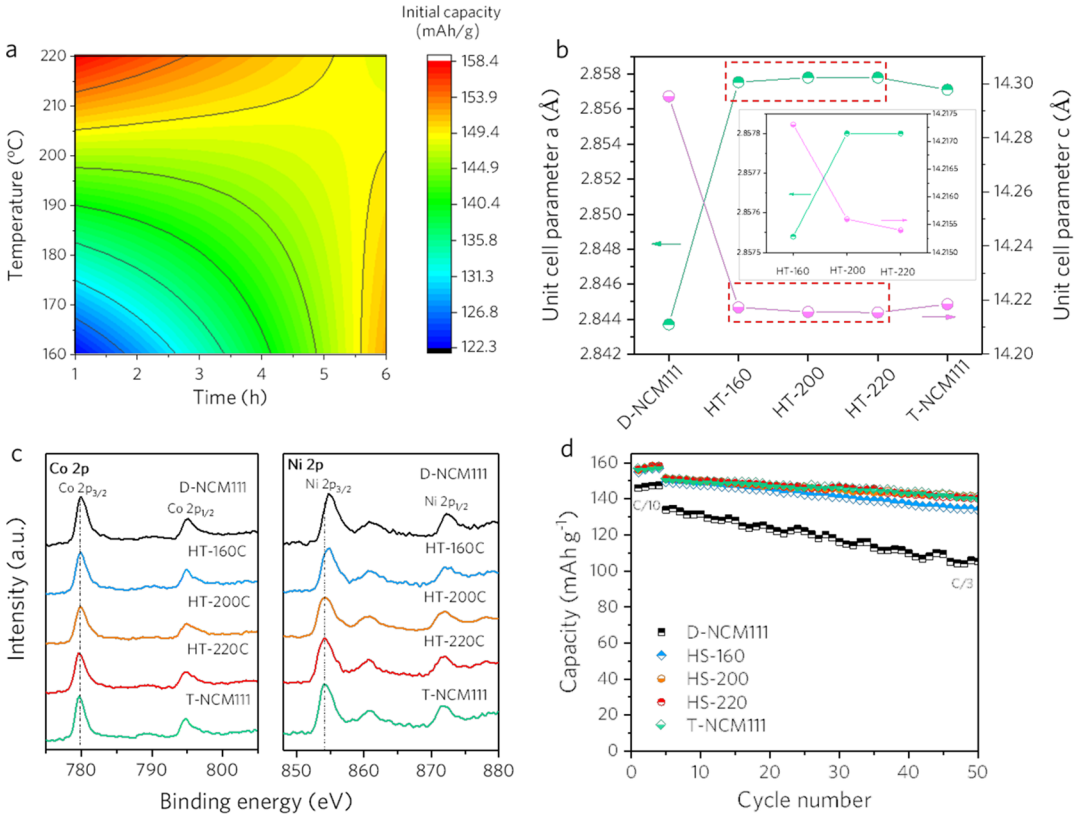

Figure 2. Investigation of temperature and time in the hydrothermal relithiation process. Contour map of the effects of hydrothermal temperature and time on initial capacity (a), unit cell parameters of *a* and *c* evolution (b), XPS spectra in Co 2p and Ni 2p regions (c), and electrochemical cycling stability (d) of samples relithiated at temperatures of 160, 200, and 220 °C and control samples (T-NCM111 and D-NCM111).

https://doi.org/10.1021/acssuschemeng.0c09017
ACS Sustainable Chem. Eng. 2021, 9, 4543−4553

only 120 mAh/g (80.5%) was retained after 50 cycles. However, when the relithiation time was increased to 2 h, the capacity at the end of the 50th cycle reached 131 mAh/g, corresponding to a retention of 87.3%. Longer treatment times, like 4 and 6 h, did not improve the cycling performance further (Table S1).

The temperature, time, and initial capacity data in Table S1 were then evaluated for underlying trends using robust polynomial regression, as described above. The polynomial that met the selection criteria was of the form, $y = a_1x_1 + a_2x_2 + b_2x_2(x_1 - x_2)$. The values of the fitting parameters are given in Table S2, which produced an r^2 greater than 0.99. From the data in Table S2, the value of a_2 is much greater than that of a_1, indicating that the hydrothermal process time was the most important factor to obtain high-performing cathode materials. The negative value of b_2, at first glance, is somewhat puzzling and indicates that the interaction of time and temperature negatively affected the initial capacity of these materials. In the time and temperature range studied, the value of $b_2x_2(x_1 - x_2)$ was always negative and tended to decrease (became more negative) with increasing time at a given temperature. Together, these observations indicated that there was an optimum value beyond which additional hydrothermal time would not be beneficial. A contour map, shown in Figure 2a, was generated from the selected polynomial to help visualize the trends in the data.

The samples that showed the highest cycling performance, 160 °C-6 h, 200 °C-6 h, and 220 °C-2 h, were selected for additional characterization. They are denoted as HT-160, HT-200, and HT-220, respectively. XRD was first performed to characterize the crystal structure (Figure S2). Overall, the samples treated at different temperatures as well as the control samples (T-NCM111 and D-NCM111) displayed the typical diffraction peaks associated with the α-$NaFeO_2$ structure ($R\bar{3}m$ space group), indicating that the bulk structure of NCM111 is not affected by chemical delithiation and relithiation.[24,25] After chemical delithiation (D-NCM111), the (003) peak clearly shifted to a lower angle, reflecting an increase in the c lattice constant due to the increased electrostatic repulsion between the oxygen layers along the c direction due to Li^+ deficiency.[26,27] After relithiation at 160, 200, and 220 °C, the (003) peak shifted back to the same position as that of T-NCM111.

The lattice parameters were determined via Rietveld refinement of the neutron diffraction pattern (Figure S3), where the evolution of the a and c unit cell parameters was plotted in Figure 2b. After chemical relithiation, the a lattice parameter of D-NCM111 decreased from 2.85761(7) Å to 2.84370(7) Å, which originates from the decrease in the average metal−metal distance that occurs upon delithiation of the structure.[28] The c lattice parameter increased from 14.2165(4) Å to 14.2953(4) Å, which is consistent with the XRD result. Overall, the values of the a and c lattice parameters after hydrothermal relithiation were close to those of pristine T-NCM111. In contrast, the a and c lattice parameters of the HT-160 sample did not reach the values of the samples treated at higher temperatures (inset of Figure 2b), likely indicating that Li^+ had not reached its equilibrium position in the lattice (Figure 1) due to kinetic limitations at low temperature.

The valence states of the transition metals are also sensitive to the concentration of Li^+ in cathode materials, which were probed via XPS. The XPS spectra of Co 2p in Figure 2c for all the samples were analogous, with two main peaks located at 779.86 and 794.99 eV corresponding to Co $2p_{3/2}$ and Co $2p_{1/2}$, respectively.[29] The absence of a satellite peak around 785 eV indicates that the valence state of Co in all the samples was 3+, which is reasonable given that only 10% of the Li^+ was extracted from the D-NMC samples, where only Ni is expected to be oxidized due to its lower redox potential.[32,33] After chemical delithiation, the main peak at 854.28 eV related to Ni $2p_{3/2}$ of T-NCM111 shifted to a higher binding energy of 854.79 eV (D-NCM111) (Figure 2c), confirming this trend and indicating that Ni was oxidized to a higher valence state.[30,31] Although the peak shifted back slightly after relithiation at 160 °C, the binding energy was still higher than that of pristine T-NCM111, implying that some Ni^{3+} still existed in the cathode material.[32,33] Notably, the peak of Ni $2p_{3/2}$ shifted back to the same position as that of the pristine T-NCM111 for the samples treated at 200 °C for 6 h and 220 °C for 2 h, suggesting that the compositional defects were completely repaired under these relithiation conditions.

To better understand the effect of hydrothermal temperature and time on the properties of the final cathode product after direct regeneration, the electrochemical cycling performance of the samples relithiated at different temperatures was evaluated in half-cells at a rate of C/10 for four cycles followed by 50 cycles at a rate of C/3 (Figure 2d). It should be mentioned that the relithiated samples were annealed with an excess 5 mol % Li_2CO_3 at 850 °C for 4 h before the electrochemical test for a fair comparison with pristine T-NCM111. The chemical extraction of Li^+ reduced the discharge capacity of the first cycle at the C/10 rate from 156.5 mAh/g to 146.1 mAh/g (T-NCM111 vs D-NCM111). When the rate was increased to C/3, D-NCM111 showed a capacity of 133.9 mAh/g and a capacity retention of 105.3 mAh/g (78.6%) was observed after 50 cycles. The initial capacities of C/3 and C/10 rates for the samples that underwent hydrothermal relithiation at 160 °C followed by annealing improved to 154.3 mAh/g and 149.5 mAh/g, respectively, suggesting that a large portion of Li deficiencies has been recovered. However, after 50 cycles, the discharge capacity was reduced to 133.6 mAh/g, which corresponds to a capacity retention of 89.4%. When the relithiation temperatures were increased to 200 and 220 °C, the C/10 discharge capacities were found to be further increased to 156.1 and 156.3 mAh/g, respectively, which are nearly the same as that of pristine T-NCM111 (156.5 mAh/g). Notably, even at the C/3 rate, initial capacities of 150.4 and 150.6 mAh/g, respectively, were achieved, reaching the level of pristine T-NCM111 (150.5 mAh/g). At the end of the 50th cycle, the retained capacities were 140.2 and 140.3 mAh/g for the samples relithiated at 200 and 220 °C, respectively, both of which were comparable to that of T-NCM111 (140.3 mAh/g). Given this performance, it was concluded that the Li deficiencies of D-NCM111 can only be fully refilled at temperatures higher than 200 °C in the limited time frames examined here. Considering the much longer time needed to achieve full relithiation at 200 °C (6 h) as compared to 220 °C (2 h), the optimal hydrothermal relithiation temperature and duration are 220 °C and 2 h, respectively.

Investigation of Solution Composition for Hydrothermal Relithiation. The effect of the lithium-bearing solution composition used in hydrothermal relithiation was then explored. In our previous work[8,10] as well as that reported by Sloop et al.,[9,12] 4 M LiOH was used as the relithiation solution. Considering the high cost of LiOH, a more-dilute LiOH solution would be preferable. In order to exclude the

https://doi.org/10.1021/acssuschemeng.0c09017
ACS Sustainable Chem. Eng. 2021, 9, 4543−4553

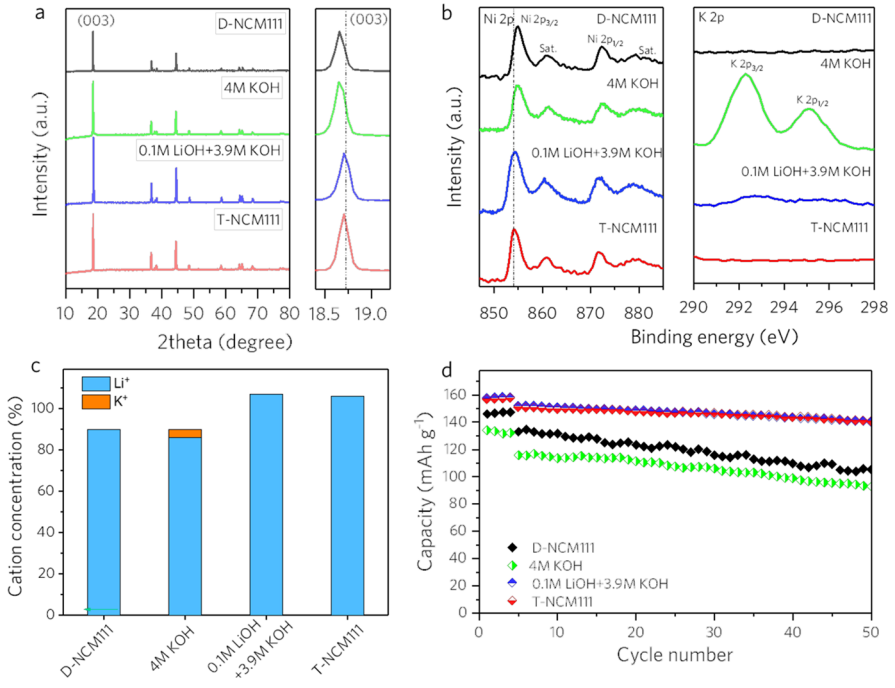

Figure 3. Investigation of solution composition for hydrothermal relithiation. XRD patterns (a), XPS spectra (b), cation (Li^+ and K^+) concentration (c), and comparison of cycling stability (d) of samples treated by the mixed solution of 0.1 M LiOH and 3.9 M KOH, and 4 M KOH and the control samples (D-NCM111 and T-NCM111).

effect of pH, a solution consisting of a mixture of 0.1 M LiOH and 3.9 M KOH (to yield 4 M OH^-) was used for relithiation.

The crystal structure of D-NCM111 that was relithiated with the mixed solution was characterized by XRD (Figure 3a). The XRD patterns of D-NCM111 and T-NCM111 as well as that treated with 4 M KOH were included as reference points. There was no evidence of any new phases present, suggesting that the layered structure of pristine T-NCM111 was maintained for all the samples. When treated with 4 M KOH, it was noted that the (003) peak presented at a lower-than-expected angle, indicating that the Li deficiencies still existed in the bulk crystal structure. However, when the 0.1 M LiOH and 3.9 M KOH solution was employed, the (003) peak returned to a position like that of pristine T-NCM111, which suggests that the structure was fully lithiated.

XPS was again performed to probe the valence state of Ni in the above samples (Figure 3b). The Ni 2p spectra of all the samples showed two main peaks corresponding to Ni $2p_{3/2}$ and Ni $2p_{1/2}$, accompanied by a satellite peak (denoted as "Sat."). The treatment with 4 M KOH did not change the peak position of the Ni $2p_{3/2}$ peak as compared to that in D-NCM111, suggesting that the valence state of Ni was still higher than that of pristine T-NCM111. This indicates that K^+ may not have appreciably intercalated into the lattice vacancies of the layered structure. By comparison, the Ni $2p_{3/2}$ peak from D-NMC111 treated with the mixed solution shifted back to the same position as that from the pristine T-NCM111, indicating that Ni was reduced to 2+. In order to further confirm the exclusion of K^+ in the mixed-solution case, XPS measurements in the K 2p binding energy region were carried out. Interestingly, two noticeable peaks related to K $2p_{3/2}$ and K $2p_{1/2}$ for the sample treated with 4 M KOH were seen (Figure 3b), which implies the intercalation and possible exchange of K^+ and Li^+. On the contrary, the sample treated with the mixed solution showed a flat XPS spectrum in this binding energy region, suggesting that there was negligible K^+ intercalation or Li^+/K^+ exchange.

The concentrations of Li^+ and K^+ in the cathode particles were further examined by ICP-MS measurement (Figure 3c). Note that the original chemical oxidation of T-NCM111 extracted 10% of the Li^+ (D-NCM111) from the pristine cathode particles. After hydrothermal treatment with the 4 M KOH solution, it was found that an additional 4% of Li^+ in the particles was lost. Meanwhile, ~4% of K^+ was detected in the cathode particles, which supports the hypothesis of Li^+/K^+ exchange proposed above. When 0.1 M LiOH was introduced, the cation exchange was eliminated and no K^+ was detected in the relithiated sample. Moreover, the Li stoichiometry of NCM111 was found to be 1.07 after treatment for 2 h, which is close to the value of T-NCM111 (1.06). The preferred insertion of Li^+ into D-NCM111 is due to its higher reduction potential (Figure S4) as well as smaller size (0.74 Å vs 1.38 Å) compared to K^+, respectively, leading to a lower thermodynamical and kinetics barrier. This result implies that the existence of a large amount of KOH in the relithiation solution does not affect the relithiation process if a small concentration of Li^+ is present in the solution.

The electrochemical performance was then evaluated to understand the effect of the mixed solution on the properties of the regenerated sample. Prior to the electrochemical test, the samples were again annealed at 850 °C for 4 h with excess 5 mol % Li_2CO_3 after hydrothermal relithiation. As shown in Figure 3d, the discharge capacity of the sample treated with 4 M KOH only produced a capacity of 134.3 mAh/g, which was even lower than that of D-NCM111 (146.1 mAh/g), which indicates that the Li^+/K^+ exchange has a detrimental effect on performance (Figure 3c). After treatment with the mixed solution, the capacity was restored to 156.4 mAh/g, which is nearly the same as that of T-NCM111 (156.5 mAh/g). At a C/3 rate, the sample treated with 4 M KOH only delivered an

https://doi.org/10.1021/acssuschemeng.0c09017
ACS Sustainable Chem. Eng. 2021, 9, 4543−4553

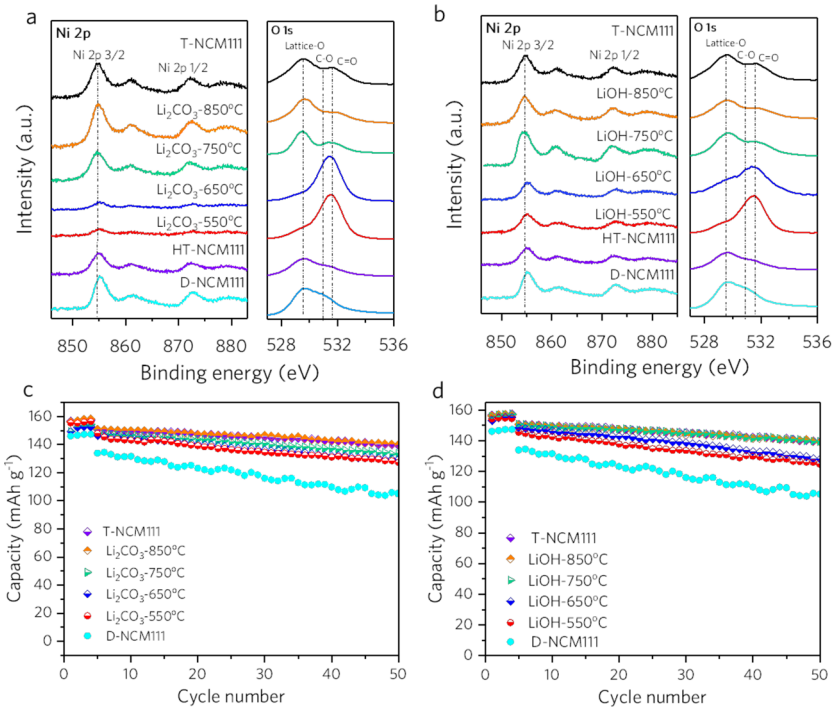

Figure 4. Investigation of the lithium source compensating for lithium loss in the annealing process. XPS spectra of relithiated samples after annealing at temperatures of 550, 650, 750, and 850 °C with Li_2CO_3 (a) and LiOH (b) as the Li source. Cycling stability of relithiated samples after annealing at temperatures of 550, 650, 750, and 850 °C with Li_2CO_3 (c) and LiOH (d) as the Li source.

initial capacity of 115.6 mAh/g, also less than that of D-NCM111 (133.9 mAh/g), which then further decayed to 92.4 mAh/g over 50 cycles. Conversely, after treatment with the mixed solution, the sample delivered an initial capacity of 150.4 mAh/g, which decreased to 140.1 mAh/g after 50 cycles. The obtained capacity retention (93.1%) was comparable to that of T-NCM111 (93.2%). The effective regeneration of D-NCM111 using the mixed solution to achieve the same level of performance as using 4 M LiOH suggests that the cathode recycling cost can be reduced by replacing a majority of Li in the relithiation solution, leading to a lower raw material cost.

It also needs to be mentioned that besides the replacement of 4 M LiOH with a mixture of 0.1 M LiOH and 3.9 M KOH, the cost of hydrothermal relithiation can be also reduced by recycling the concentrated LiOH solution. To briefly evaluate the process effectiveness, a D-NMC111 sample was relithiated with a previously used 4 M LiOH solution at 220 °C for 2 h, annealed at 850 °C, and subjected to electrochemical cycling for comparison. The initial discharge capacities of the sample were found to be 156.6 and 150.5 mAh/g at C/10 and C/3, respectively, also retaining 92.8% of this capacity after 50 cycles, comparable to that of T-NCM111 (Figure S5). The viability of continuous recycle/reuse of the spent LiOH during relithiation also represents a promising strategy in reducing the recycling cost based on the hydrothermal relithiation method.

Investigation of the Lithium Source Compensating for Lithium Loss in the Annealing Process. After hydrothermal relithiation, a short annealing is required to remedy the remaining structural defects and achieve the desired electrochemical performance (Figure 1). However, during high-temperature annealing, a portion of Li in the crystal structure will be lost,[34,35] leading to inferior capacity and cycling instability (Figure S6). Generally, 5 mol % excess of Li is added to compensate for Li loss in this step.[36,37] The effects of annealing temperatures on the composition and electrochemical performance of the final regenerated NCM111 were explored when Li_2CO_3 and LiOH were used as the Li source. Figure 4a shows the XPS spectra of samples annealed with Li_2CO_3 at different temperatures. In the XPS spectra for Ni, the position of the main Ni $2p_{3/2}$ peak was not affected by the annealing temperature and remained almost identical to that of the pristine T-NCM111 for all the samples. Nevertheless, the peak intensity relative to O 1s increased significantly with increased annealing temperature. The relatively low intensity of the samples annealed at low temperatures, such as 550 and 650 °C, might be due to the undecomposed Li_2CO_3, which reduced the signal from the underlying crystalline NCM111.[38] This was supported by the O 1s XPS spectra, where the intensity of the peak associated with lattice oxygen almost disappeared for the sample annealed at 550 and 650 °C. Additionally, the cumulative intensity of the peaks related to C−O and C═O was quite high, which suggests that a large portion of Li_2CO_3 was still present on the surface. When the annealing temperature was increased to 750 °C, however, the intensity of the lattice oxygen peak increased and the intensity of the peak associated with Li_2CO_3 decreased, indicating that the additional Li was incorporated into the crystal structure of NCM111. This incorporation was further increased when the annealing temperature was increased to 850 °C.

When LiOH was used as the Li source instead, the relative intensity ratio of Ni 2p to O 1s for the samples annealed at 550 and 650 °C was not as low as that for the sample annealed with Li_2CO_3 under the same conditions (Figure 4b). This result indicates that some Li^+ was incorporated into the material at lower temperatures, likely due to the lower melting point of LiOH (471 °C) than Li_2CO_3 (723 °C),[39] and is consistent with a recent work by Dahn et al.[40] They found that the typical

https://doi.org/10.1021/acssuschemeng.0c09017
ACS Sustainable Chem. Eng. 2021, 9, 4543−4553

(003) peak of layered cathode materials started to appear at ~575 °C when LiOH was used as the Li precursor, whereas it emerged at ~775 °C when Li_2CO_3 was used as the Li precursor. In the O 1s spectra, the signals of C−O and C═O associated with Li_2CO_3 are likely due to the reaction of CO_2 and surface LiOH when the sample was exposed to air.[38,41] When the annealing temperature was increased to 750 °C, the intensity of the peak associated with the lattice oxygen was increased while that of Li_2CO_3 decreased. The relative intensity of the peaks did not change when the relithiated sample was annealed at 850 °C, similar to that of pristine T-NCM111.

The electrochemical performances of the samples annealed at different conditions were then compared with the same protocol described earlier. When the relithiated sample was annealed at 550 °C, the capacity of the first charging cycle at C/10 was 231.4 mAh/g (Figure S7), far beyond that of pristine T-NCM111 (182.8 mAh/g). The discharge capacity was only 154.6 mAh/g, corresponding to a Coulombic efficiency (CE) of 66.8%, which again is likely from the irreversible Li^+ capacity introduced by residual Li_2CO_3.[42] However, after washing with water, the charge capacity dropped to 185.4 mAh/g (Figure S8), indicating that the additional capacity originated from the residual Li_2CO_3. When the annealing temperature was increased to 650 °C, the charge and discharge capacities dropped to 212.2 and 152.3 mAh/g, respectively, corresponding to a CE of 71.7%, indicating that the inactive Li_2CO_3 remained in the cathode material. Even when the temperature was further increased to 750 °C, the charge capacity was still as high as 206.4 mAh/g but the discharge capacity was only 149.8 mAh/g. When the annealing temperature was increased to 850 °C, the charge capacity dropped to 182.2 mAh/g and the discharge capacity increased to 156.8 mAh/g, achieving a CE of 86.1%, which is even higher than that of pristine T-NCM111 (85.6%).

The cycling stability was also compared for these samples annealed with Li_2CO_3 at various temperatures (Figure 4c) and is summarized in Table S3. The samples annealed at 550 and 650 °C showed a similar capacity degradation trend where the capacity retention was improved from 88.2% to 90.4%. Increasing the annealing temperature to 850 °C further increased the initial capacity to 150.4 mAh/g and a capacity of 140.7 mAh/g could be achieved after 50 cycles (a capacity retention of 93.1%), which is comparable to pristine T-NCM111. Therefore, it was concluded that 850 °C is the minimum temperature required for fully restoring the electrochemical performance of D-NCM111 when Li_2CO_3 is used as the Li source.

The optimal annealing time was studied as well at 850 °C, where the cycling stability of relithiated samples annealed at 850 °C for 1, 2, 4, and 6 h is shown in Figure S9. After annealing for 1 h, the sample exhibited a capacity of 149.1 mAh/g, which decreased to 130.2 mAh/g over 50 cycles. With a further increase in annealing time to 2 h, the initial capacity was not affected dramatically (150.2 mAh/g). Nevertheless, the capacity after 50 cycles was improved to 135.6 mAh/g, which increased further to 140.3 mAh/g when the sample was annealed for 4 h. However, annealing for 6 h did not improve the capacity or cycling stability. Therefore, a duration of 4 h is sufficient to attain the desirable electrochemical performance.

Due to the lower melting point (471 °C),[40] LiOH was proposed as an alternative to Li_2CO_3. Similarly, different annealing temperatures were explored to identify the optimal temperature for fully recovering the electrochemical properties of the regenerated cathode. When the annealing temperature was 550 °C, the charge capacity reached 180.3 mAh/g (Figure S10), which was significantly lower than that of the sample annealed under the same condition with Li_2CO_3 as the Li source (231.4 mAh/g). The reversible capacity was 154.4 mAh/g, corresponding to a CE of 85.6%. This indicates that Li^+ from LiOH can be more easily incorporated into the layered crystal structure at a low temperature compared to that from Li_2CO_3. The charge and discharge capacities did not change when the temperature was increased to 650 °C. The increase in temperature to 750 °C improved the reversible capacity to 156.7 mAh/g, almost identical to that of the sample annealed at 850 °C (156.8 mAh/g).

The cycling stability of all the samples annealed with LiOH is shown in Figure 4d, and the results are summarized in Table S3. The samples annealed at 550 and 650 °C delivered initial capacities of 145.4 and 148.2 mAh/g, respectively, at a C/3 rate. After 50 cycles, capacities of 124.6 and 128.3 mAh/g were measured, corresponding to capacity retentions of 85.6% and 86.5%, respectively. When the temperature was increased to 750 °C, the capacity increased to 150.5 mAh/g and 93.2% of this capacity was retained after 50 cycles. Notably, the capacity and retention were nearly the same as those of the sample annealed at 850 °C. The 750 °C annealing temperature produced a similar performance to that of the pristine T-NCM111, 100 °C less than that required when annealing with Li_2CO_3. It appears that although a relatively low temperature can trigger the incorporation of LiOH, the temperature must still be high enough to obtain a phase that can withstand long-term charge/discharge cycling. Nevertheless, the optimal annealing temperature could be decreased from 850 to 750 °C when Li_2CO_3 was replaced by LiOH as a Li source.

The T-NCM and R-NCM electrodes after 50 cycles were characterized by XPS and XRD to probe the difference in structural durability. The overall survey XPS spectra of the cycled T-NCM and R-NCM (Figure S11a) showed additional signals of F and P compared with that of the pristine T-NCM, which originate from the formed cathode electrolyte interphase (CEI) on the cycled cathode particles after cycling. The high-resolution Ni 2p XPS spectra (Figure S11b) displayed a similar right shift for both the cycled T-NCM and R-NCM electrodes, indicating a higher valence state of Ni, which is resulted from the loss of the active Li^+ after cycling. The XRD diffraction peaks in Figure S11c matched well with the layered structure, and no major phase impurity was detected for the cycled materials. Overall, no appreciable difference in terms of structure and composition was observed between R-NCM and T-NCM after cycling.

Additionally, the direct regeneration was scaled up from 1 to 10 g of cathode per batch to demonstrate the viability of the process. The composition of the product (R-NCM-10 g) was analyzed by ICP (Table S4), where the Li content was found to be similar to that of T-NCM111, showing no difference from the sample regenerated at a smaller scale (R-NCM-1 g). R-NCM-10 g was further characterized by XRD and XPS. Compared with the starting D-NCM, a right shift of the (003) diffraction peak (Figure S12a) and a left shift of the Ni $2p_{3/2}$ peak (Figure S12b) similar to those observed for the R-NCM-1 g sample were also present for the R-NCM-10 g sample, suggesting that the recovery of the structure and composition is not affected by the increase in the material loading in the relithiation reactor. Moreover, both the capacity (Figure S2c)

https://doi.org/10.1021/acssuschemeng.0c09017
ACS Sustainable Chem. Eng. 2021, 9, 4543−4553

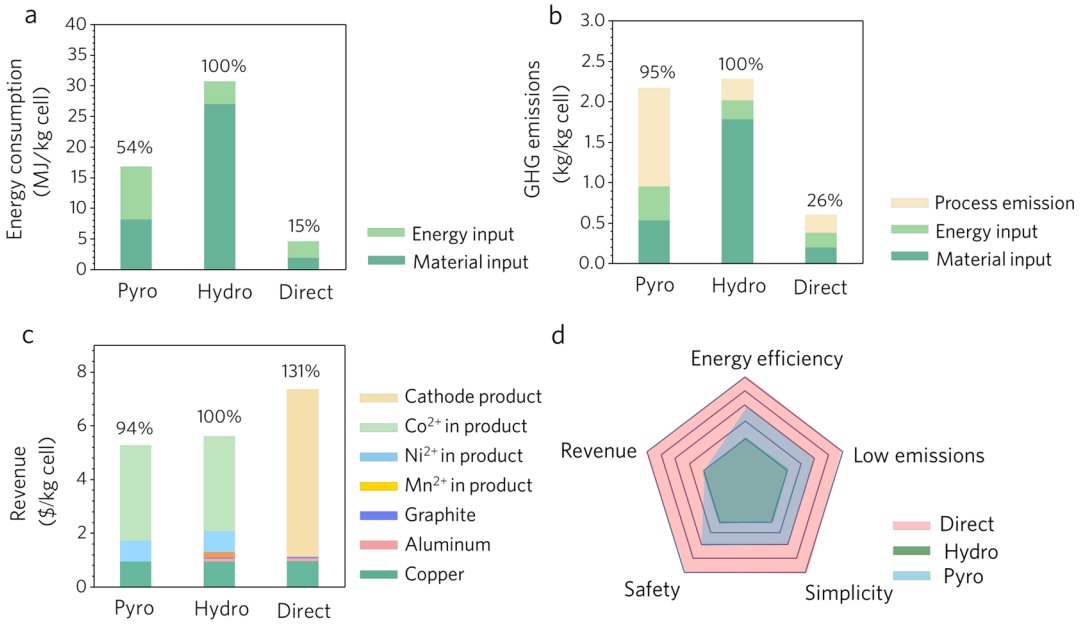

Figure 5. Life cycle anaysis of pyrometallurgical (Pyro), hydrometallurgical (Hydro), and direct (Direct) recycling methods. Energy consumption (a), GHG emissions (b), potential revenue from outputs produced (c), and spider chart comparing various features (d) of Pyro, Hydro, and Direct recycling methods.

and retention (Figure S12d) of R-NCM-10 g were found to be identical to those of the pristine level (T-NCM111), indicating the scalability of this process for industrial application.

Life Cycle Analysis of Pyrometallurgical, Hydrometallurgical, and Direct Recycling Methods. The environmental and economic impacts of the direct regeneration process were evaluated with the EverBatt model[43] and were compared with those of commercialized pyrometallurgical (Pyro) and hydrometallurgical (Hydro) recycling methods. A detailed description of the methodology can be found in the Supporting Information. It should be noted that the energy consumption and greenhouse gas (GHG) emissions as well as the recycling cost and revenue related to Pyro and Direct recycling were normalized to the counterpart of Hydro, as it is the most widely applied technology for the current recycling industry.

In terms of cumulative energy consumption (Figure 5a), Hydro was projected to consume the highest energy, which is mainly due to its large amount of material input (dark green bar). Regarding the entire life cycle analysis, the EverBatt model takes the energy consumed in the upstream manufacturing processes of these chemicals into consideration. When only the energy input (light green bar) in the recycling processing itself was considered, the energy consumed in Pyro was projected to be higher than that in hydrometallurgy because of the high temperature required in the smelting step. Evidently, the dominant factors attributed to the modeling results are related primarily to raw material input and equipment. In the direct recycling method (Direct), the only consumed raw material is LiOH, of which the amount is determined by the Li loss of the spent cathode materials. In this regard, the concentrated KOH or LiOH solution can be recycled and reused as demonstrated above. Moreover, direct recycling avoided the demand for high-energy-consuming equipment like that needed in pyrometallurgy. Therefore, fewer chemicals and milder processing conditions enabled direct recycling to have energy consumption as low as 4.5 MJ for recycling 1 kg of spent LIBs, which was only 15% of that for hydrometallurgy.

For GHG emissions, both pyro- and hydrometallurgy exhibited higher projected emissions compared with the direct recycling method (Figure 5b). The GHG emissions of pyrometallurgy are mainly from the recycling process (smelting), but the upstream manufacturing of chemicals contributes much of the total GHG emissions from hydrometallurgy. Notably, for the direct recycling of 1 kg of spent LIBs, only 0.6 kg of GHG was released, which is significantly lower than those of pyrometallurgy (2.16 kg) and hydrometallurgy (2.27 kg).

Besides the low energy consumption and GHG emissions, the direct regeneration process is projected to produce the highest revenue (Figure 5c) because the recycled cathode output can be directly used to produce new LIBs, which are more valuable than the precursors produced in pyro- and hydrometallurgy. The regenerated cathode production (light yellow bar) promises to translate into $5.80 with a total revenue of $6.90. However, for pyro- and hydrometallurgical recycling, cathodes are broken down into elemental products. While Ni and Co precursors are highly valuable, the total revenues for pyro- and hydrometallurgy are projected to be only $5.20 and $5.60, respectively. It should be mentioned that both pyro- and hydrometallurgical recycling end with Ni/Co/Mn precursors in the EverBatt model, which means that additional resynthesis steps for producing cathode materials are required. If the final products of pyro- and hydrometallurgy are the same as that obtained from the direct recycling, the energy consumption and GHG emissions would undoubtedly be higher than those shown in Figure 5.

A comprehensive comparison of different recycling methods is illustrated in the spider chart (Figure 5d). In terms of energy efficiency, emissions, and revenue, the advantages of the direct recycling method were clear based on the results shown in Figure 5a–c. Furthermore, as direct recycling does not involve high temperatures above 1000 °C nor uses large amounts of

https://doi.org/10.1021/acssuschemeng.0c09017
ACS Sustainable Chem. Eng. 2021, 9, 4543−4553

corrosive acid/alkaline chemicals, we believe that it is also advantageous for safety. Additionally, considering the procedures of the three recycling methods (Figures S13–S15), the operation of direct recycling was relatively simple, avoiding multiple leaching and precipitation steps. Therefore, the direct regeneration embodies the "4H" principle,[2] namely, high efficiency, high economic return, high environmental benefit, and high safety.

CONCLUSIONS

In summary, the effect of hydrothermal relithiation processing parameters on the properties of the cathode materials from direct recycling was investigated. During this investigation, it was found that hydrothermal relithiation at 220 °C for 2 h is optimal in terms of balancing operation temperature and time. Additionally, the relithiation solution of 4 M LiOH, extensively used in previous studies, can be replaced with a more cost-effective mixed solution consisting of 0.1 M LiOH and 3.9 M KOH to achieve the same quality cathode. Alternatively, it was demonstrated that the concentrated 4 M LiOH solution can be recycled and reused for relithiation without sacrificing the material properties. Both of these strategies can potentially lower the regeneration costs associated with raw material input. As for the annealing step, it was found that the optimal temperature can be reduced from 850 to 750 °C when Li_2CO_3 was replaced by LiOH, which can effectively reduce energy consumption and CO_2 exhaust in the recycle process. Further verification of the effectiveness of our regeneration process by scaling from 1 to 10 g of cathode per batch as well as compliance with the "4H" principle demonstrates the promise of hydrothermal relithiation-based direct regeneration for industrial application.

ASSOCIATED CONTENT

Supporting Information

The Supporting Information is available free of charge at https://pubs.acs.org/doi/10.1021/acssuschemeng.0c09017.

Effects of relithiation temperature and time on the electrochemical performance and crystal structure (Figures S1–S3 and Tables S1 and S2); CV curves of D-NCM in aqueous LiOH and KOH solutions; verification of the recyclability of LiOH solution (Figure S5); necessity of the additional Li source during the annealing step (Figure S6); effects of annealing temperature and time on the electrochemical performance (Figures S7–S10 and Table S3); composition and structure comparison of cycled pristine and relithiated NCM111 electrodes (Figure S11); validation of the scalability of the regeneration process (Figure S12 and Table S4); and methodology of the life cycle analysis of recycling methods (Figures S13–S15 and Tables S5 and S6) (PDF)

AUTHOR INFORMATION

Corresponding Author

Zheng Chen − *Department of NanoEngineering, Program of Materials Science, Sustainable Power and Energy Center, and Program of Chemical Engineering, University of California, San Diego, La Jolla, California 92093, United States;* orcid.org/0000-0002-9186-4298; Email: zhengchen@eng.ucsd.edu

Authors

Panpan Xu − *Department of NanoEngineering, University of California, San Diego, La Jolla, California 92093, United States;* orcid.org/0000-0001-7277-9920

Zhenzhen Yang − *Chemical Sciences and Engineering Division, Argonne National Laboratory, Lemont, Illinois 60439, United States*

Xiaolu Yu − *Program of Materials Science, University of California, San Diego, La Jolla, California 92093, United States*

John Holoubek − *Department of NanoEngineering, University of California, San Diego, La Jolla, California 92093, United States;* orcid.org/0000-0003-0015-4512

Hongpeng Gao − *Program of Materials Science, University of California, San Diego, La Jolla, California 92093, United States*

Mingqian Li − *Department of NanoEngineering, University of California, San Diego, La Jolla, California 92093, United States*

Guorui Cai − *Department of NanoEngineering, University of California, San Diego, La Jolla, California 92093, United States*

Ira Bloom − *Chemical Sciences and Engineering Division, Argonne National Laboratory, Lemont, Illinois 60439, United States;* orcid.org/0000-0002-4877-473X

Haodong Liu − *Department of NanoEngineering, University of California, San Diego, La Jolla, California 92093, United States*

Yan Chen − *Neutron Scattering Division, Oak Ridge National Laboratory, Oak Ridge, Tennessee 37830, United States*

Ke An − *Neutron Scattering Division, Oak Ridge National Laboratory, Oak Ridge, Tennessee 37830, United States*

Krzysztof Z. Pupek − *Applied Materials Division, Argonne National Laboratory, Lemont, Illinois 60439, United States*

Ping Liu − *Department of NanoEngineering, Program of Materials Science, Sustainable Power and Energy Center, and Program of Chemical Engineering, University of California, San Diego, La Jolla, California 92093, United States;* orcid.org/0000-0002-1488-1668

Complete contact information is available at: https://pubs.acs.org/10.1021/acssuschemeng.0c09017

Author Contributions

Z.C., convinced of the idea, designed the experiment and directed the project. P.X. carried out the synthesis, processing, and electrochemical evaluations and analyzed the data. H.L. assisted with neutron diffraction characterization. Z.Y. and I.B. performed XPS measurement and modeling. H.P., M.L., G.C., and P.L. revised the manuscript. All authors discussed the results and commented on the manuscript.

Notes

The authors declare the following competing financial interest(s): A Patent was filed for this work through the UCSD Office of Innovation and Commercialization.

ACKNOWLEDGMENTS

We gratefully acknowledge support from US Department of Energy (DOE) via the ReCell Center, Vehicle Technologies Office, specifically from Samuel Gillard, and David Howell. Neutron diffraction work was carried out at the Spallation Neutron Source (SNS), which is the U.S. Department of Energy (DOE) user facility at the Oak Ridge National

Laboratory, sponsored by the Scientific User Facilities Division, Office of Basic Energy Sciences. A majority of cell fabrication and electrochemical testing was performed in the UCSD-MTI Battery Fabrication and the UCSD-Arbin Battery Testing Facility. This work was performed in part at the San Diego Nanotechnology Infrastructure (SDNI) of UCSD, a member of the National Nanotechnology Coordinated Infrastructure, which is supported by the National Science Foundation (grant ECCS-1542148). The submitted manuscript has been partially created by UChicago Argonne, LLC, Operator of Argonne National Laboratory ("Argonne"). Argonne, a U.S. Department of Energy Office of Science laboratory, is operated under contract no. DE-AC02-06CH11357. The U.S. Government retains for itself, and others acting on its behalf, a paid-up nonexclusive, irrevocable worldwide license in said article to reproduce, prepare derivative works, distribute copies to the public, and perform publicly and display publicly, by or on behalf of the Government. The Department of Energy will provide public access to these results of federally sponsored research in accordance with the DOE Public Access Plan. http://energy.gov/downloads/doe-public-access-plan

REFERENCES

(1) Chen, M.; Ma, X.; Chen, B.; Arsenault, R.; Karlson, P.; Simon, N.; Wang, Y. Recycling end-of-life electric vehicle lithium-ion batteries. *Joule* **2019**, *3*, 2622−2646.

(2) Fan, E.; Li, L.; Wang, Z.; Lin, J.; Huang, Y.; Yao, Y.; Chen, R.; Wu, F. Sustainable recycling technology for Li-ion batteries and beyond: Challenges and future prospects. *Chem. Rev.* **2020**, *120*, 7020−7063.

(3) Zhang, X.; Li, L.; Fan, E.; Xue, Q.; Bian, Y.; Wu, F.; Chen, R. Toward sustainable and systematic recycling of spent rechargeable batteries. *Chem. Soc. Rev.* **2018**, *47*, 7239−7302.

(4) Lv, W.; Wang, Z.; Cao, H.; Sun, Y.; Zhang, Y.; Sun, Z. A critical review and analysis on the recycling of spent lithium-ion batteries. *ACS Sustainable Chem. Eng.* **2018**, *6*, 1504−1521.

(5) Ciez, R. E.; Whitacre, J. F. Examining different recycling processes for lithium-ion batteries. *Nat. Sustainability* **2019**, *2*, 148−156.

(6) Wang, H.; Friedrich, B. Development of a highly efficient hydrometallurgical recycling process for automotive Li-ion batteries. *J. Sustainable Metall.* **2015**, *1*, 168−178.

(7) Yun, L.; Linh, D.; Shui, L.; Peng, X.; Garg, A.; Le, M. L. P.; Asghari, S.; Sandoval, J. Metallurgical and mechanical methods for recycling of lithium-ion battery pack for electric vehicles. *Resour., Conserv. Recycl.* **2018**, *136*, 198−208.

(8) Shi, Y.; Chen, G.; Chen, Z. Effective regeneration of $LiCoO_2$ from spent lithium-ion batteries: a direct approach towards high-performance active particles. *Green Chem.* **2018**, *20*, 851−862.

(9) Sloop, S.; Crandon, L.; Allen, M.; Koetje, K.; Reed, L.; Gaines, L.; Sirisaksoontorn, W.; Lerner, M. A direct recycling case study from a lithium-ion battery recall. *Sustainable Mater. Technol.* **2020**, *25*, No. e00152.

(10) Shi, Y.; Chen, G.; Liu, F.; Yue, X.; Chen, Z. Resolving the compositional and structural defects of degraded $LiNi_xCo_yMn_zO_2$ particles to directly regenerate high-performance lithium-ion battery cathodes. *ACS Energy Lett.* **2018**, *3*, 1683−1692.

(11) Shi, Y.; Zhang, M.; Meng, Y. S.; Chen, Z. Ambient-pressure relithiation of degraded $Li_xNi_{0.5}Co_{0.2}Mn_{0.3}O_2$($0 < x < 1$) via eutectic solutions for direct regeneration of lithium-ion battery cathodes. *Adv. Energy Mater.* **2019**, *9*, 1900454.

(12) Sloop, S. E.; Crandon, L.; Allen, M.; Lerner, M. M.; Zhang, H.; Sirisaksoontorn, W.; Gaines, L.; Kim, J.; Lee, M. Cathode healing methods for recycling of lithium-ion batteries. *Sustainable Mater. Technol.* **2019**, *22*, No. e00113.

(13) Pillot, C. In *The Rechargeable Battery Market And Main Trends 2018−2030*; Advanced Automotive Battery Conference, Pillot, C., Ed., 2019.

(14) Myung, S.-T.; Maglia, F.; Park, K.-J.; Yoon, C. S.; Lamp, P.; Kim, S.-J.; Sun, Y.-K. Nickel-Rich Layered Cathode Materials for Automotive Lithium-Ion Batteries: Achievements and Perspectives. *ACS Energy Lett.* **2017**, *2*, 196−223.

(15) An, K.; Wang, X. L.; Stoica, A. D. *VDRIVE- data reduction and interactive visualization software for event mode neutron diffraction*; 1521−3773; 2012; p 621.

(16) Toby, B. H. EXPGUI, a graphical user interface for GSAS. *J. Appl. Cryst.* **2001**, *34*, 210−213.

(17) Liu, H.; Liu, H.; Lapidus, S. H.; Meng, Y. S.; Chupas, P. J.; Chapman, K. W. Sensitivity and Limitations of Structures from X-ray and Neutron-Based Diffraction Analyses of Transition Metal Oxide Lithium-Battery Electrodes. *J. Electrochem. Soc.* **2017**, *164*, A1802−A1811.

(18) Scheffé, H. Experiments with Mixtures. *J. R. Stat. Soc. Ser. B* **1958**, *20*, 344−360.

(19) Scheffé, H. The Simplex-Centroid Design for Experiments with Mixtures. *J. R. Stat. Soc. Ser. B* **1963**, *25*, 235−251.

(20) Behrens, J. T. Principles and procedures of exploratory data analysis. *Psychol Methods* **1997**, *2*, 131−160.

(21) Holland, P. W.; Welsch, R. E. Robust regression using iteratively reweighted least-squares. *Commun. Stat. Theory Methods* **1977**, *6*, 813−827.

(22) Stuart, M. Understanding Robust and Exploratory Data Analysis. *J. R. Stat. Soc. Ser. D* **1984**, *33*, 320−321.

(23) Sahore, R.; Peebles, C.; Abraham, D. P.; Gilbert, J.; Bloom, I. Additive effects in high-voltage layered-oxide cells: A statistics of mixtures approach. *J. Power Sources* **2017**, *362*, 342−348.

(24) Ross, B. J.; LeResche, M.; Liu, D.; Durham, J. L.; Dahl, E. U.; Lipson, A. L. Mitigating the Impact of Thermal Binder Removal for Direct Li-Ion Battery Recycling. *ACS Sustainable Chem. Eng.* **2020**, *8*, 12511−12515.

(25) Liu, H.; Liu, H.; Seymour, I. D.; Chernova, N.; Wiaderek, K. M.; Trease, N. M.; Hy, S.; Chen, Y.; An, K.; Zhang, M.; Borkiewicz, O. J.; Lapidus, S. H.; Qiu, B.; Xia, Y.; Liu, Z.; Chupas, P. J.; Chapman, K. W.; Whittingham, M. S.; Grey, C. P.; Meng, Y. S. Identifying the chemical and structural irreversibility in $LiNi_{0.8}Co_{0.15}Al_{0.05}O_2$ - a model compound for classical layered intercalation. *J. Mater. Chem. A* **2018**, *6*, 4189−4198.

(26) Mohanty, D.; Kalnaus, S.; Meisner, R. A.; Rhodes, K. J.; Li, J.; Payzant, E. A.; Wood, D. L., III; Daniel, C. Structural transformation of a lithium-rich $Li_{1.2}Co_{0.1}Mn_{0.55}Ni_{0.15}O_2$ cathode during high voltage cycling resolved by in situ X-ray diffraction. *J. Power Sources* **2013**, *229*, 239−248.

(27) Liu, H.; Chen, Y.; Hy, S.; An, K.; Venkatachalam, S.; Qian, D.; Zhang, M.; Meng, Y. S. Operando Lithium Dynamics in the Li-Rich Layered Oxide Cathode Material via Neutron Diffraction. *Adv. Energy Mater.* **2016**, *6*, 1502143.

(28) Kim, J.-M.; Chung, H.-T. Role of transition metals in layered $Li[Ni,Co,Mn]O_2$ under electrochemical operation. *Electrochim. Acta* **2004**, *49*, 3573−3580.

(29) Rustomji, C. S.; Yang, Y.; Kim, T. K.; Mac, J.; Kim, Y. J.; Caldwell, E.; Chung, H.; Meng, Y. S. Liquefied gas electrolytes for electrochemical energy storage devices. *Science* **2017**, *356*, No. eaal4263.

(30) Jia, H.; Zhu, W.; Xu, Z.; Nie, X.; Liu, T.; Gao, L.; Zhao, J. Precursor effects on structural ordering and electrochemical performances of Ni-rich layered $LiNi_{0.8}Co_{0.2}O_2$ cathode materials for high-rate lithium ion batteries. *Electrochim. Acta* **2018**, *266*, 7−16.

(31) Carroll, K. J.; Qian, D.; Fell, C.; Calvin, S.; Veith, G. M.; Chi, M.; Baggetto, L.; Meng, Y. S. Probing the electrode/electrolyte interface in the lithium excess layered oxide $Li_{1.2}Ni_{0.2}Mn_{0.6}O_2$. *Phys. Chem. Chem. Phys.* **2013**, *15*, 11128−11138.

(32) Larcher, D.; Palacín, M. R.; Amatucci, G. G.; Tarascon, J.-M. Electrochemically active $LiCoO_2$ and $LiNiO_2$ made by cationic

https://doi.org/10.1021/acssuschemeng.0c09017
ACS Sustainable Chem. Eng. 2021, 9, 4543−4553

exchange under hydrothermal conditions. *J. Electrochem. Soc.* **1997**, *144*, 408.
(33) Radin, M. D.; Hy, S.; Sina, M.; Fang, C.; Liu, H.; Vinckeviciute, J.; Zhang, M.; Whittingham, M. S.; Meng, Y. S.; Van der Ven, A. Narrowing the gap between theoretical and practical capacities in Li-Ion layered oxide cathode materials. *Adv. Energy Mater.* **2017**, *7*, 1602888.
(34) Arai, H.; Okada, S.; Ohtsuka, H.; Ichimura, M.; Yamaki, J. Characterization and cathode performance of $Li_{1-x}Ni_{1+x}O_2$ prepared with the excess lithium method. *Solid State Ionics* **1995**, *80*, 261−269.
(35) Caurant, D.; Baffier, N.; Garcia, B.; Pereira-Ramosb, J. P. Synthesis by a soft chemistry route and characterization of $LiNi_xCo_{1-x}O(0 < x < 1)$ cathode materials. *Solid State Ionics* **1996**, *91*, 45−54.
(36) Yao, X.; Xu, Z.; Yao, Z.; Cheng, W.; Gao, H.; Zhao, Q.; Li, J.; Zhou, A. Oxalate co-precipitation synthesis of $LiNi_{0.6}Co_{0.2}Mn_{0.2}O_2$ for low-cost and high-energy lithium-ion batteries. *Mater. Today Commun.* **2019**, *19*, 262−270.
(37) Xu, X.; Huo, H.; Jian, J.; Wang, L.; Zhu, H.; Xu, S.; He, X.; Yin, G.; Du, C.; Sun, X. Radially oriented single-crystal primary nanosheets enable ultrahigh rate and cycling properties of $LiNi_{0.8}Co_{0.1}Mn_{0.1}O_2$ cathode material for lithium-ion batteries. *Adv. Energy Mater.* **2019**, *9*, 1803963.
(38) You, Y.; Celio, H.; Li, J.; Dolocan, A.; Manthiram, A. Modified High-Nickel Cathodes with Stable Surface Chemistry Against Ambient Air for Lithium-Ion Batteries. *Angew. Chem., Int. Ed.* **2018**, *57*, 6480−6485.
(39) Beyer, H.; Meini, S.; Tsiouvaras, N.; Piana, M.; Gasteiger, H. A. Thermal and electrochemical decomposition of lithium peroxide in non-catalyzed carbon cathodes for Li−air batteries. *Phys. Chem. Chem. Phys.* **2013**, *15*, 11025−11037.
(40) Weber, R.; Li, H.; Chen, W.; Kim, C.-Y.; Plucknett, K.; Dahn, J. R. In situ XRD studies during synthesis of single-crystal $LiNiO_2$, $LiNi_{0.975}Mg_{0.025}O_2$, and $LiNi_{0.95}Al_{0.05}O_2$ cathode materials. *J. Electrochem. Soc.* **2020**, *167*, 100501.
(41) Xie, Q.; Manthiram, A. Long-life, ultrahigh-nickel cathodes with excellent air storage stability for high-energy density lithium-based batteries. *Chem. Mater.* **2020**, *32*, 7413−7424.
(42) Julien, C.; Mauger, A.; Zaghib, K.; Groult, H. Optimization of layered cathode materials for lithium-ion batteries. *Materials* **2016**, *9*, 595.
(43) Dai, Q.; Gaines, L.; Spangenberger, J.; Kelly, J. C.; Ahmed, S.; Wang, M. *EverBatt: A closed-loop battery recycling cost and environmental impacts model*. www.anl.gov/egs/everbatt, p. 2019.

https://doi.org/10.1021/acssuschemeng.0c09017
ACS Sustainable Chem. Eng. 2021, 9, 4543−4553